

COMPUTATIONAL COMPARATIVE STUDY FOR DESIGN OF LOW REYNOLDS NUMBER AIRFOIL

Katsutoshi KONDO*

***Department of Mechanical Engineering, Tokyo University of Science, Tokyo, Japan
kondo@flab.isas.jaxa.jp**

Keywords: *Aerodynamic Characteristics, CFD, Low Reynolds Number Flow, Airfoil*

Abstract

Aerodynamic characteristics of several symmetric and asymmetric airfoils are investigated using two-dimensional laminar simulations at the Reynolds number of 23,000 to identify geometric features of airfoil with high aerodynamic performance. The definitions of high aerodynamic performance in this study are 1) high lift-to-drag ratio, 2) linear lift slope, and 3) longitudinal static stability.

Comparisons of the symmetric airfoils suggest that a thin airfoil has a linear $C_l - \alpha$ and larger degree of a lift slope than a thick airfoil. On the other hand, for asymmetric airfoils, high cambered airfoils attain greater the lift but increase the drag without a flat upper surface. In addition, the flat upper surface decreases the drag due to suppression of the separated region. As the common aerodynamic characteristics of the all airfoils, negative $dC_{mp}/d\alpha$ cannot be attained consistently at the all angles of attack. Current study has pointed out: 1) High lift-to-drag ratio airfoil can be obtained by making the airfoil with camber and flat upper surface; 2) Thin and flat upper surface leads to linear lift slope and low drag; and 3) the movement of separation bubble on the upper surface and increase of the suction peak with the angle of attack causes the difficulty of attaining longitudinal static stability

1 Introduction

Development of Micro Air Vehicles (MAVs) and Unmanned Air Vehicles (UAVs) has been an active research area. These vehicles are able to conduct many important missions such as

environmental monitoring, planetary exploration, and search and rescue operation in natural disasters. In our laboratory, Mars atmosphere exploration using a fixed-wing UAV has been considered and studied in this decade. An atmospheric density of Mars is one hundredth of the Earth. In addition, the chord length of a main wing of the UAV is roughly 0.5 meters due to the limitation of the transportation capsule. Consequently, flight Reynolds number of the UAV on Mars becomes the order of 10^4 . Under such low Reynolds number conditions, flow-fields are often shown complicated flow phenomenon (e.g. flow-fields involve separation, transition, and sometimes reattachment) so that aerodynamic performance of airfoils, which are generally utilized under high Reynolds number conditions, drastically degrades [1]. Therefore, it is important to understand the aerodynamic characteristics in low Reynolds number regime and many studies have been carried out.

Kojima et al. [2] have showed flow and aerodynamic characteristics of NACA0002 and NACA0012 using three-dimensional large-eddy simulations (3D-LES). Uranga et al. [3] and Galbraith et al. [4] have investigated the flow features around the SD7003 airfoil using 3D-LES. In above analysis, flow characteristics over the airfoil under low Reynolds number conditions have been well discussed. For analysis of low Reynolds number flow, unsteady and high-accuracy simulations such as 3D-LES are preferable because it is required to accurate estimate the separation, transition, and reattachment. Recently, Anyoji et al. [5] have discussed the aerodynamics characteristics of the high performance airfoils at low Reynolds

number with both CFD and experiment approaches. They have provided the useful knowledge for the design of low Reynolds number airfoils. However, limited discussion regarding the pitching moment behavior has been made in previous efforts.

When the new airfoil is designed, some criteria of the required aerodynamic characteristics are determined like high lift, low drag, stall characteristics, pitching moment behavior and so forth. As the next step, preferred tools for the design of airfoil are selected for example, parametric study using CFD or EFD with a lot of trial and error, numerical optimization and so forth. Sasaki et al. [6] conduct optimization of airfoil at the fixed Reynolds number and angle of attack. This study considers only enhancement of the lift-to-drag ratio and does not consider the robustness or pitching moment behavior.

Then, current study performs the parametric study with relatively low-cost two-dimensional laminar simulations. The objective of the current study is to find what geometric features of airfoil attain high aerodynamic performance under low Reynolds number condition. There might be a lot of criterions of the high aerodynamic performance of airfoils of the UAVs. Current study considers following three aerodynamic characteristics as the criteria of the high aerodynamic performance;

- 1) High lift-to-drag ratio,
- 2) Linear lift slope,
- 3) Longitudinal static stability.

It is well known that the high lift-to-drag ratio airfoil could perform an efficient cruise flight. The lift slope becomes important when aerodynamic control is concerned. The longitudinal static stability is directly related to the aerodynamic stability.

Parametric study is conducted using 2D-Laminar simulations at the fixed Reynolds number. Several airfoils including bio-inspired and engineering airfoils are chosen in order to discuss the effects of airfoil thickness and camber on the above-mentioned aerodynamic characteristics and find aerodynamically preferable geometric feature of the airfoil for the fixed-wing based low Reynolds number aircrafts.

2 Computational Setup

2.1 Computational Condition

Following ten airfoils considered in this study are selected based on geometric feature of the airfoil; symmetric airfoils (NACA0003, NACA0006, NACA0009, and NACA0012) and asymmetric airfoils (NACA5505, NACA64A204, SD7003, and Ishii, cross-sectional owl and seagull wing). The owl and seagull airfoils are constructed by the formula given by Liu et al. ($z/b = 0.4$). [7]

The freestream Mach number is set to be 0.2 at which compressibility can be ignored and computational efficiency can be improved. Chord-length-and freestream-based Reynolds number is set to be 23,000. The angle of attack ranges from -9.0 to 9.0 degrees.

2.2 Computational Methods

All simulations are performed with two-dimensional laminar simulations (2D-Laminar) by using LANS3D developed in ISAS/JAXA. The two-dimensional compressible Navier-Stokes equations normalized by chord length and sound speed (a_∞) at freestream and generalized in curvilinear coordinates are employed as the governing equations. The spatial derivatives of convective and viscous terms, metrics, and Jacobians are evaluated by the sixth-order compact difference scheme [8] with tenth order filter (filter coefficient is 0.495) [9] for numerical stability. For time-integration, the second-order backward difference of alternating directional implicit symmetric Gauss-Seidel implicit method [10] with five-times sub-iterations [11] in each time step is adopted. The computational time (dt) normalized by chord length and sound speed is $2.5 \times 10^{-4} c/a_\infty$ in non-dimensional time, so that the maximum Courant-Friedrichs-Lewy number becomes approximately 1.5. At the boundary all variables are extrapolated from one point inside of the outflow boundary. On the airfoil surface, non-slip conditions are adopted.

2.3 Computational Mesh and Boundary Conditions

As an example computational grid around NACA0006 is illustrated in figure 1. C-type structure mesh is utilized for the computational mesh. Grid coordinates are oriented such that ξ traverses clockwise around the airfoil and η is normal to the surface. Computational mesh consists of 615x101 points in ξ, η directions, respectively, which is approximately 62 thousand points in total. The first grid points away from the airfoil surface are fixed for all grids and set to be $0.03c/\sqrt{Re}$. The farfield boundary is positioned $30c$ away from the airfoil in order to reduce its influence on the solution near the airfoil. At the outflow boundary, all variables are extrapolated from one point inside of the outflow boundary. On the airfoil surface non-slip adiabatic wall boundary condition is adopted.

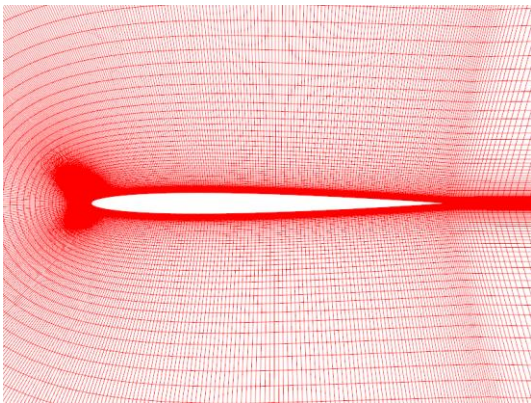


Fig. 1. Computational grid (NACA0006).

3 Results and Discussion

3.1 Validation and Verification

Firstly, validity of 2D-Laminar is discussed by comparing with the results of experiments and three-dimensional large-eddy simulations (3D-LES). Lift coefficients and surface pressure distribution of the Ishii airfoil are compared. For the comparing data, results of 3D-LES and experiments obtained by Anyoji et al. [5] are adopted.

Figure 2 shows the comparison of lift coefficient. Lift coefficients of 2D-Laminar well agree with 3D-LES and experiments at the angle

of attack ranging from 0.0 to 4.5 degrees. When the angle of attack exceeds 4.5 degrees, slight differences among 2D-Laminar, 3D-LES, and experiments are seen. Furthermore, it is found that the stall angle is different in all methods. This fact suggests that estimation of the stall angle is difficult using both CFD and experiment methods at the Reynolds number of 23,000 because the stall behavior strongly depends on accurate capturing laminar separation bubble. Note that this study does not discuss the stall behavior near the angle of attack of 9.0 degrees.

Figure 3 illustrates the surface pressure distributions at the angles of attack of (a) 3.0, (b) 6.0, and (c) 9.0 degrees. At the angle of attack of 3.0 degrees (figure 3(a)), the surface pressure coefficient of 2D-Laminar agrees well with that of 3D-iLES because the flow over the airfoil is basically laminar. Experimental results also well agree with 2D-Laminar. At the angle of attack of 6.0 degrees, the results are almost agreement in that of the experiment and the 3D-LES except for secondary peak observed near $x/c=0.4$ and the increase of the surface pressure coefficient near $x/c=0.5$ on the suction side. This secondary peak of surface pressure on the suction side also has been presented in Uranga et al. study [3]. When the angle of attack becomes 9.0 degrees, the secondary peak is more significantly observed near $x/c=0.3$. As a result, the surface pressure coefficient of 2D-laminar differs from other methods.

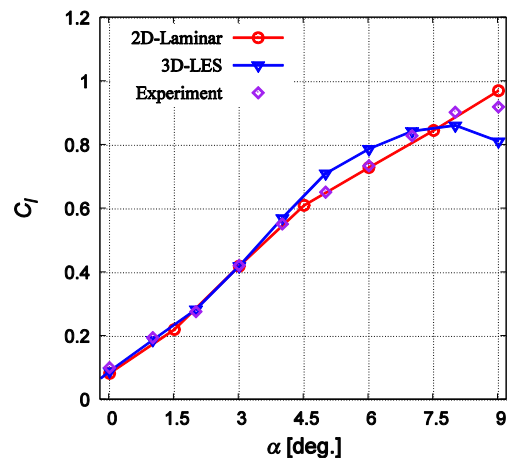


Fig. 2. Comparison of lift coefficients among 2D-Laminar (red), 3D-LES (blue), and experiments (purple).

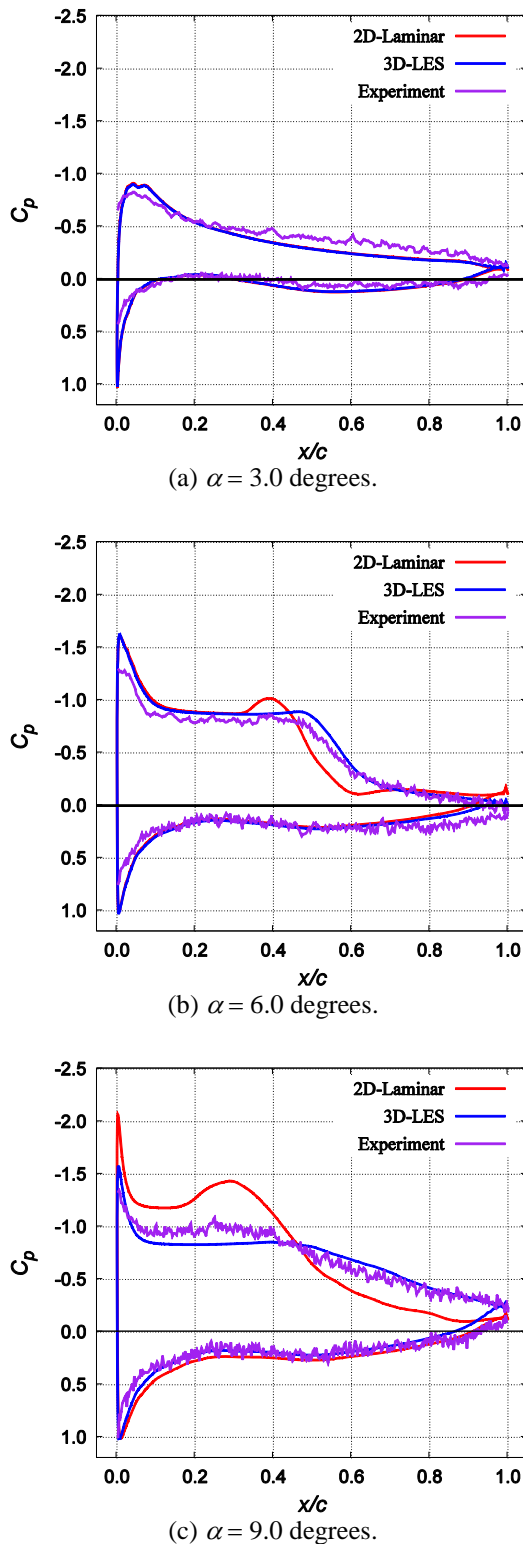


Fig. 3. Comparison of surface pressure coefficients at the angle of attack of (a) 3.0 degrees, (b) 6.0 degrees, (c) 9.0 degrees.

3.2 Aerodynamics of Symmetric Airfoils

Effects of thickness of symmetric airfoils on the aerodynamic characteristics are discussed in this section. Aerodynamic coefficients of four

airfoils are compared; NACA0003, NACA0006, NACA0009, and NACA0012. Comparison of airfoil geometries are shown in figure 4. Lift and pitching moment coefficients, and drag polar curves are plotted in figure 5 and 6, respectively. Note that aerodynamic characteristics at only positive angles of attack are compared due to symmetric airfoils.

Lift coefficient of thin airfoil is clearly larger than that of thick airfoil at low angles of attack ($\alpha = 0.0 - 3.0[\text{deg.}]$). As the angle of attack increases, the order becomes almost same. The linear lift slope of NACA0003 is observed at the all angles of attack considered in this work. The lift slope is slightly smaller than 2π which is calculated by a thin airfoil theory. Lift curves of airfoils except for NACA0003 show nonlinearity when the angle of attack varies from 3.0 to 4.5 degrees. This nonlinearity of the lift slope is unique characteristics due to laminar separation bubble in the low Reynolds number regime. The variations of lift coefficients between the angle of attack of 3.0 and 4.5 degrees are more significant with increasing thickness of the airfoil.

The drag coefficient of the airfoils indicates the opposite characteristics to the lift coefficient. The drag coefficient of thin airfoil is smaller at the low angles of attack, but that is higher at the high angles of attack than that of thick airfoil. In order to understand sharp rise of the drag coefficients, the drag coefficient is decomposed into pressure and viscous drag. These forces are depicted in figure 7. For each airfoil the viscous drag is consistently same order. On the other hand, the pressure drag denotes the same tendency of the total drag and is an order of magnitude greater than viscous drag. Generally, it implies that separated region have a greater impact on the total drag when the pressure drag is relatively greater than the viscous drag. It is noticeable that induced drag and wave drag generated by tip vortices and compressible flow is ignorable because this study considers two-dimensional airfoil. From these factors, it is important for the design of the airfoil to make the separated region small in low Reynolds number regime.

Next, pitching moment coefficients at the quarter chord from the leading-edge are

compared. Moment coefficients of all airfoils are nearly zero at low angles of attack, but slightly increase. After that generation and movement of the laminar separation bubble toward leading edge side influence the pitching moment behavior, subsequently, which become corrugated distribution with the angle of attack. As a result, moment slopes of the all airfoils do not keep $dC_{mp}/d\alpha < 0$.

Finally, lift-to-drag ratio is discussed and summarized the effects of thickness. Maximum lift-to-drag ratio for each airfoil is presented in table 1. NACA0006 and NACA0009 attain 15 of maximum lift-to-drag ratio at the angle of attack of 4.5 degrees that are highest value in this work. In addition, taking nonlinearity of the lift slope and drag polar into account, airfoil thickness of 6% is preferable for the Reynolds number considered in this study (NACA0006). However, moment slope of the all airfoil do not keep negative $dC_{mp}/d\alpha$.

3.3 Aerodynamics of Asymmetric Airfoils

In this section, aerodynamics of asymmetric airfoils is discussed. Here, the asymmetric airfoils are grouped based on the degree of camber of the airfoil. First one corresponds relatively large cambered airfoils (NACA5505, owl, and seagull airfoils) and second one corresponds to slightly cambered airfoils (NACA64A204, SD7003, and Ishii airfoils) and discussed about each group.

3.3.1 Large Cambered Airfoils

The airfoil geometries with large camber are shown in figure 8. The seagull airfoil consists of deeply concaved lower surface and great convex upper surface. The maximum thickness and camber of the seagull airfoil is 9.7% at $x/c = 0.20$ and 10.0 % at $x/c = 0.44$, respectively. The owl also possesses concaved lower surface but its upper surface is relatively flat in comparison

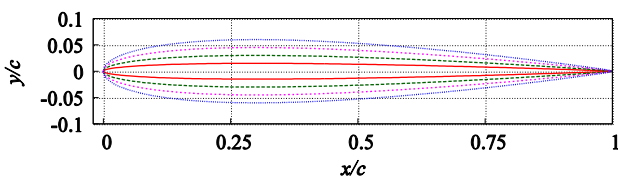


Fig. 4. Geometry of symmetric airfoils. (red : NACA0003, green : NACA0006, purple : NACA0009, and blue : NACA0012).

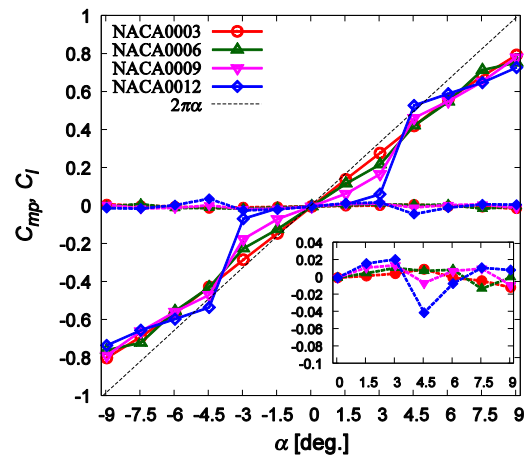


Fig. 5. Lift and pitching moment coefficients. Solid and broken line indicates lift and pitching moment coefficients, respectively.

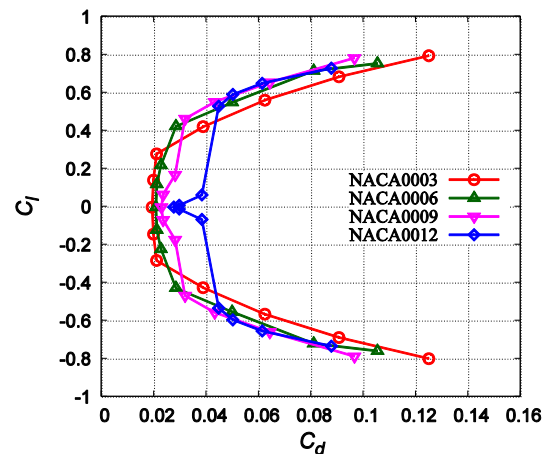


Fig. 6. Drag polar curve.

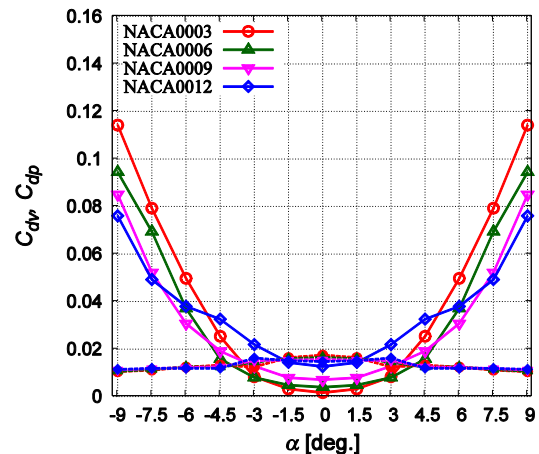


Fig. 7. Decomposition of drag coefficients. Solid and broken lines indicate pressure and viscous drag, respectively.

Table 1. Maximum lift-to-drag ratios.

	NACA0003	NACA0006	NACA0009	NACA0012
L/D	13	15	15	12

with the other two airfoils. The maximum thickness and camber of the owl airfoil is 5.5% at $x/c = 0.11$ and 4.9% at $x/c = 0.47$, respectively. NACA5505 has smaller camber on the both upper and lower surface than seagull airfoil. Considering these geometric features, aerodynamic characteristics of cambered airfoils are compared and discussed.

Lift and pitching moment coefficients are shown in figure 9 with those of NACA0006 for the reference. All airfoils show higher lift coefficients than $C_l = 2\pi\alpha$. Especially, the seagull airfoil shows much higher lift coefficient than the other airfoils. The NACA5505 and owl airfoils also gain higher lift coefficients than NACA0006. Nonlinearity of lift slopes can be observed in each airfoil at the different angle of attack. For the seagull airfoil, remarkable nonlinearity can be seen at the angle of attack between 0.0 to 3.0 degrees. NACA5505 and the owl airfoils also show the nonlinear lift slopes. For these airfoils different reasons from the seagull airfoils are pointed out. To understand this nonlinearity of the $C_l - \alpha$ curve, surface pressure coefficients of the owl airfoil at the angle of attack between 3.0 and 6.0 degrees are depicted in figure 10. Slightly nonlinearity can be seen in lift slope of the owl airfoil at the angle of attack between 1.5 and 3.0 degrees. It occurs by weakening of the pressure plateau on the lower surface at $x/c = 0.2 \sim 0.65$ due to the laminar separation bubble. Strong nonlinearity in the lift slope of the seagull airfoil is due to this factor even though the effects of airfoil thickness also include. Some airfoils with the laminar separation bubble on the lower surface show nonlinearity like the seagull airfoil and others do not indicate it like NACA5505. The relationship between nonlinear lift slope and separation bubble on the lower surface is in progress. On the other hand, nonlinearity of the lift slope at the angle of attack between 3.0 and 4.5 degrees is caused by pressure plateau on the upper surface due to generating the laminar separation bubble. This tendency can be observed in $C_l - \alpha$ curve of almost all of the airfoils except for NACA0003 and it is difficult to remove this effect in low Reynolds number regime. The reason why the laminar separation bubble have been used to the advantage for the

lift enhancement but initially include nonlinear behavior.

Drag polar curves of the cambered airfoils are shown in figure 11. Drag coefficients of the airfoils are increased as the camber is enlarged. As camber is enlarged, separated region increases. Subsequently, as mentioned above, the pressure drag is dominant factor for the total drag in Reynolds number considered in this study so that the pressure drag increases. Therefore, it is necessary to be paid attention to the upper surface geometry to suppress the pressure drag.

The pitching moment coefficients of cambered airfoils are larger negative than NACA0006 as shown in figure 9. Generally, large cambered airfoil leads to large negative nose-down pitching moment. Here, it should be noticed that a vertical axis in enlarged view of the pitching moment coefficients in figure 9 is different from that of figure 5. However, as shown in figure 9, change of the pitching moment slope can be seen as twice in the all airfoils. In addition, the pitching moment for the owl airfoil at the angle of attack of 6.0 and NACA5505 at the angle of attack of 7.5 degrees has a hump. This hump comes into existence by drastically movement toward leading edge side. As shown in figure 10, pressure plateau exists on the near the trailing edge at the angle of attack of 4.5 degree. When the angle of attack becomes 6.0 degrees, the pressure plateau moves toward leading edge side. The pressure plateau corresponds to the location of the laminar separation bubble, so that this fact indicates that the hump occurs due to the movement of the laminar separation bubble. This phenomena is possible to occur any airfoil on which the laminar separation bubble exists.

Finally, Lift-to-drag ratio is discussed. Table 2 indicates maximum lift-to-drag ratio for each airfoil. From the comparison of the maximum lift-to-drag, the owl airfoil attains 23 that is the highest maximum lift-to-drag ratio in this study. On the other hand, the seagull airfoil possesses 13 of the maximum lift-to-drag ratio that is the worst value though it has the deepest camber in this study. In general, the camber leads to better aerodynamic characteristics because of increase in lift generation, even

though drag also increases. However, the findings presented in this work suggest that the airfoil with large camber increases lift but does not always increase lift-to-drag ratio because of increasing separated region. In order to gain a larger lift-to-drag ratio, it is necessary not only to design a deeply concaved lower surface but also to cogitate the geometry on the upper surface. Furthermore, cambered airfoils have large negative pitching moment. In addition, $dC_{mp}/d\alpha$ of the all airfoils does not consistently become negative. In next section, the importance of the upper surface geometry is highlighted through discussions about slightly camber airfoils.

3.3.2 Small cambered Airfoils

The airfoils with small camber are illustrated in figure 12. NACA64A204 is designed for emphasizing maximizing laminar flow. NACA6A series foils are typical transonic airfoils. Note that NACA64A204 has maximum thickness of 4.0% at $x/c = 0.40$ with maximum camber of 1.3% at $x/c = 0.50$. SD7003 (Selig-Donovan 7003) airfoil is designed for low bubble drag at low Reynolds numbers. This airfoil has a maximum thickness and camber of 8.4% and 1.5%, respectively. An Ishii airfoil is designed by Mr. Ishii who had a world record of endurance time of non-propulsive flight. This airfoil has a maximum thickness and camber of 7.1% at $x/c = 1$ and 2.3% at $x/c = 0.62$.

Lift and pitching moment of the small cambered airfoils are plotted in figure 13. The magnitude of the lift in all airfoils has almost same though slightly difference can be seen at high angles of attack. However, there are differences in the nonlinearity of the lift slopes.

The lift slope of the SD7003 airfoil has a relatively stronger nonlinearity in comparison with the other two airfoils. This is because of generating the laminar separation bubble on the upper surface as mentioned above. On the other hand, NACA64A204 and the Ishii airfoils show relatively weak nonlinear lift slopes. From the comparison of the airfoil geometries in figure 12,

Table. 2. Maximum lift-to-drag ratios.

	NACA5505	Owl	Seagull
L/D	22	23	12

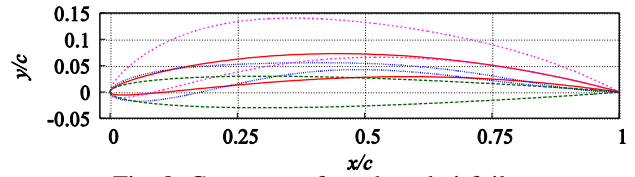


Fig. 8. Geometry of cambered airfoils. (red : NACA5505, blue : owl airfoil, purple : seagull airfoil, and green : NACA0006)

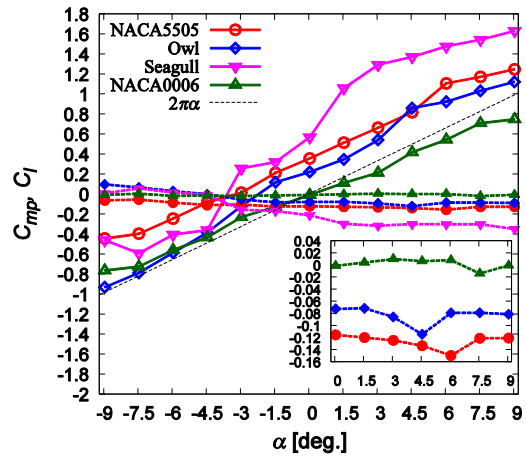


Fig. 9. Lift and pitching moment.

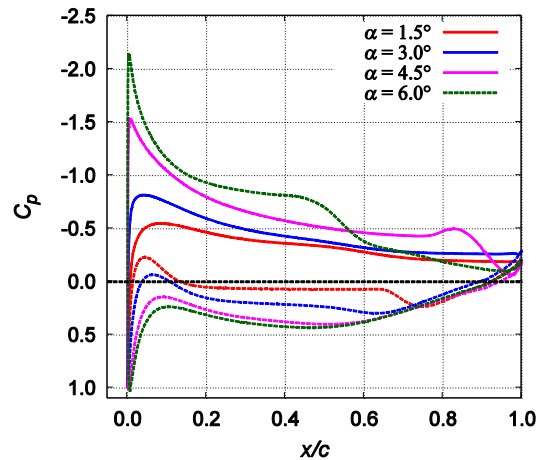


Fig. 10. Surface pressure coefficients of the owl airfoil.

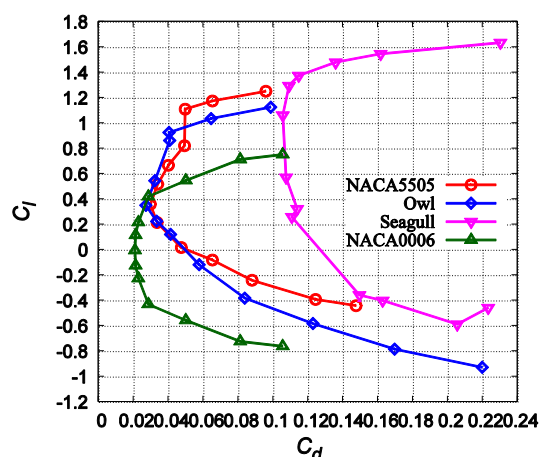


Fig. 11. Drag polar curve.

the SD7003 airfoil has more rounded upper surface compared with NACA64A204 and the Ishii airfoils. It is considered that the flatness of the upper surface is an important parameter to decrease the magnitude of the nonlinearity of the lift slope even if the laminar separation bubble is formed on the upper surface.

Drag polar curves are shown in figure 14. From the comparison of the drag polar curves, the drag of NACA64A204 and the Ishii airfoils demonstrate the same order of NACA0006. On the other hand, when the lift coefficient of SD7003 airfoil indicates nearly 0.4, the drag coefficient is approximately 0.01 higher than that of the Ishii airfoil despite of slightly difference of upper surface geometry. This fact denotes that the upper surface geometry is the significant factor for not only the lift slopes but also the magnitude of the drag.

Next, the behavior of the pitching moment is discussed. As well as the large cambered airfoil, the pitching moment of small cambered airfoils are also negative nose-down behavior. Also, the pitching moment for the SD7003 airfoil has a hump at the angle of attack of 7.5 degrees as well as it for NACA5505 and the owl airfoils can be seen. This hump is, again, due to the movement of the laminar separation bubble toward the leading edge side. The other airfoils also show the hump of the pitching moment but the magnitude is week. Furthermore, the variation of the pitching moment of the NACA64A204 and Ishii airfoils to the angle of attack is small. However, it should be noted here that $dC_{mp}/d\alpha$ of the airfoils considered in this study are not consistently negative at the angle of attack at which the laminar separation bubble is generated. This fact suggests that it is difficult to keep longitudinal static stability at the cruising angles of attack if a vehicle flies in the Reynolds number flow.

At last, maximum lift-to-drag ratios of the airfoils are compared in table 3. Comparing the lift-to-drag ratio, NACA64A204 and the Ishii airfoil attain higher maximum lift-to-drag ratio. Generally, aerodynamic performance of conventional airfoils drastically degrades [1]. Therefore, it is interesting that NACA64A204, which is typically transonic airfoil, shows as high lift-to-drag ratio as the Ishii airfoil, which

is high performance at low Reynolds number. [5] This result suggests that airfoil with “flat upper surface” can gain higher lift-to-drag ratio even if the airfoil is usually used in high Reynolds number region. From above discussion, flat upper surface is key factor to gain the high lift-to-drag ratio induced by the low drag.

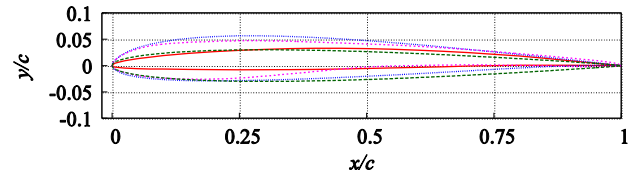


Fig. 12. Geometry of general airfoils. (red : NACA64A204, blue : SD7003, purple : Ishii, and green : NACA0006)

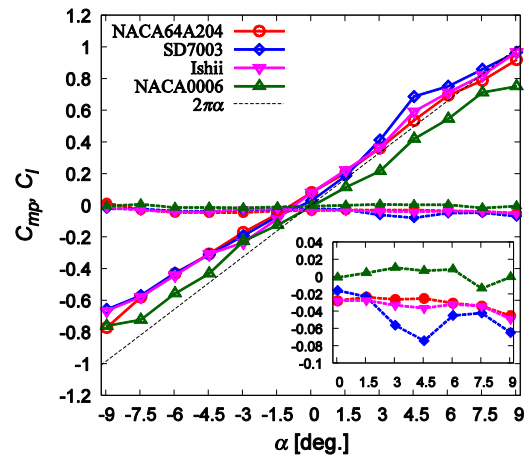


Fig. 13. Lift and pitching moment coefficients

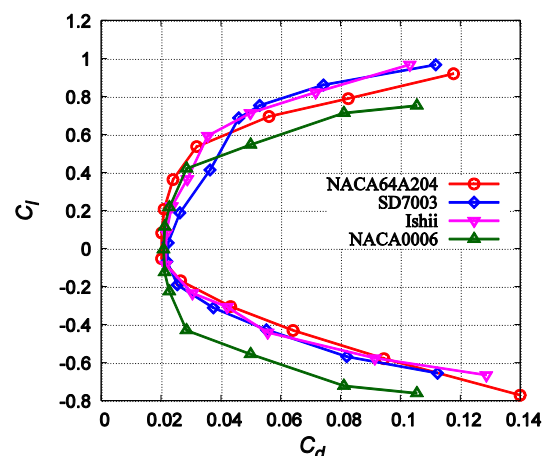


Fig. 14. Drag polar curve

Table. 3. Maximum lift-to-drag ratios.

	NACA64A204	SD7003	Ishii
L/D	17	15	17

4 Conclusions

Numerical comparative study with two-dimensional laminar simulations is conducted to investigate geometric features of airfoil with high aerodynamic performance. Several airfoils are considered at a chord based Reynolds number of 23,000 and the angle of attack ranging from -9.0 to 9.0 degrees. Definitions of high aerodynamic performance airfoil in this study are (1) high lift-to-drag ratio, (2) linear lift curve, and (3) longitudinal static stability. Above three characteristics are important parameters in design of airfoils of air vehicles. In order to understand these characteristics, aerodynamics of several symmetric and asymmetric airfoils (large and small cambered airfoil) are compared.

Comparisons of the symmetric airfoils suggest that a thin airfoil has a linear $C_l - \alpha$ and larger degree of a lift slope than a thick airfoil. In addition, analysis of the decomposition of total drag into pressure and viscous drag indicates that the pressure drag is dominant. Therefore, it is important for the design of the airfoil to make the separated region small in low Reynolds number regime.

In analysis of aerodynamics of asymmetric airfoils, asymmetric airfoils are grouped based on the degree of the camber of airfoil as small and large cambered airfoils. Aerodynamics of the cambered airfoils suggests that the degree of camber is found to have a large influence on the magnitude of the lift and negative nose-down pitching moment as well as increase the drag. The key factor to reduce the drag is flat geometry on the upper surface because magnitude of drag is determined by the size of the separated region. In addition, flat upper surface not only leads to reduction of the pressure drag but also suppresses the strength of the nonlinear lift slope.

Overall, what is common aerodynamic characteristics to all the airfoils are nonlinearity of the lift curve, hump of the pitching moment behavior, and inconsistently negative $dC_{mp}/d\alpha$. First one can be suppressed by the flatness of the upper surface. However, the other problems might not be able to be removed only excogitation of the airfoil geometry.

In summary, enhancement of the lift-to-drag ratio can be achieved by making airfoil with camber and flat upper surface. Thin airfoil thickness and flat upper surface prevent nonlinearity of lift slope. It is difficult to keep longitudinal static stability due to moving separation bubble and increasing suction peak with the angle of attack.

References

- [1] Lissaman P B S. Low-Reynolds-number airfoils. Annual Review of Fluid Mechanics, Vol. 15, pp. 223-239, 1983.
- [2] Kojima R, Nonomura T, Oyama A, Fujii K. Large-Eddy Simulation of Low-Reynolds-Number Flow Over Thick and Thin NACA Airfoils. Journal of Aircraft, Vol. 50, No. 1, 2013.
- [3] Uranga A, Persson P -O, Drela M, Peraire J. Implicit Large Eddy Simulation of transition to turbulence at low Reynolds numbers using a Discontinuous Galerkin method. International Journal for Numerical Methods in Engineering, Vol. 87, Issue 1-5, pp. 232-261, 2011.
- [4] Galbraith C M, Visbal R M. Implicit Large Eddy Simulation of Low-Reynolds-Number Transitional Flow Past SD7003 Airfoil. 40th Fluid Dynamics Conference and Exhibit, Chicago, Illinois, AIAA 2010-4737, 2010.
- [5] Anyoji, M., Nonomura, T., Aono, H., Oyama, A., Fujii, K., Nagai, H. & Asai, K. Computational and Experimental Analysis of a High Performance Airfoil under Low-Reynolds-Number Flow Condition. Journal of Aircraft, Accepted.
- [6] Sasaki G, Itakura K, Tatsukawa T, Nonomura T, Yonemoto K, Oyama A, Matsumoto T. Multi-Objective Optimization of Airfoil for Mars Exploration Aircraft Using Genetic Algorithm. 29th International Symposium on Space Technology and Science, Nagoya, Japan, 2013-k-5, 2013.
- [7] Liu T, Kuykendoll K, Rhew R, Jones S. Avian Wing Geometry and Kinematics, AIAA Journal, vol.44, No.5, pp. 954-963, 2006.
- [8] Lele S K. Compact Finite Difference Scheme with Spectral-Like Resolution, Journal of Computational Physics, Vol.103, Issue 1, pp. 16-42, 1992.
- [9] Gaitonde D V, Visbal R M. Pade-type high-order boundary filters for the navier-stokes equations. AIAA Journal, Vol. 38, No.11, pp. 2103-2112, 2000.
- [10] Nishida H, Nonomura T. Adi-sgs scheme on ideal magnetohydrodynamics. Journal of Computational Physics, 228, pp. 3182-3188, 2009.
- [11] Chakravarthy S R. Relaxation Methods for Unfactored Implicit Upwind Schemes. AIAA Paper 84-0165, 1984.

Copyright Statement

The authors confirm that they, and/or their company or organization, hold copyright on all of the original material included in this paper. The authors also confirm that they have obtained permission, from the copyright holder of any third party material included in this paper, to publish it as part of their paper. The authors confirm that they give permission, or have obtained permission from the copyright holder of this paper, for the publication and distribution of this paper as part of the ICAS 2014 proceedings or as individual off-prints from the proceedings.